

Oscillatory Neural Network-Based Ising Machine Using 2D Memristors

Xi Chen,[#] Dongliang Yang,[#] Geunwoo Hwang,[#] Yujiao Dong, Binbin Cui, Dingchen Wang, Hegan Chen, Ning Lin, Wenqi Zhang, Huihan Li, Ruiwen Shao, Peng Lin, Heemyoung Hong, Yugui Yao, Linfeng Sun,^{*} Zhongrui Wang,^{*} and Heejun Yang^{*}



Cite This: <https://doi.org/10.1021/acsnano.3c10559>



Read Online

ACCESS |

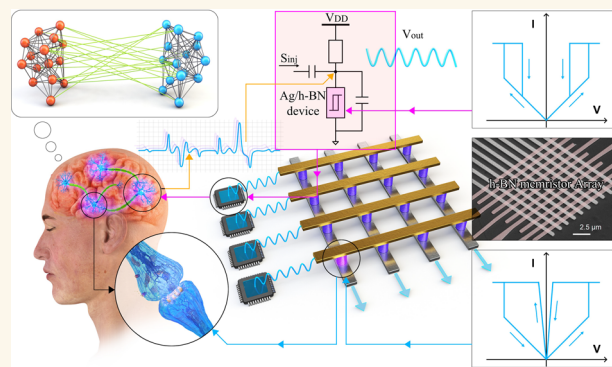
Metrics & More

Article Recommendations

Supporting Information

ABSTRACT: Neural networks are increasingly used to solve optimization problems in various fields, including operations research, design automation, and gene sequencing. However, these networks face challenges due to the nondeterministic polynomial time (NP)-hard issue, which results in exponentially increasing computational complexity as the problem size grows. Conventional digital hardware struggles with the von Neumann bottleneck, the slowdown of Moore's law, and the complexity arising from heterogeneous system design. Two-dimensional (2D) memristors offer a potential solution to these hardware challenges, with their in-memory computing, decent scalability, and rich dynamic behaviors. In this study, we explore the use of nonvolatile 2D memristors to emulate synapses in a discrete-time Hopfield neural network, enabling the network to solve continuous optimization problems, like finding the minimum value of a quadratic polynomial, and tackle combinatorial optimization problems like Max-Cut. Additionally, we coupled volatile memristor-based oscillators with nonvolatile memristor synapses to create an oscillatory neural network-based Ising machine, a continuous-time analog dynamic system capable of solving combinatorial optimization problems including Max-Cut and map coloring through phase synchronization. Our findings demonstrate that 2D memristors have the potential to significantly enhance the efficiency, compactness, and homogeneity of integrated Ising machines, which is useful for future advances in neural networks for optimization problems.

KEYWORDS: memristor, in-memory computing, crossbar array, Ising machine, combinatorial optimization



INTRODUCTION

The rapid development of artificial intelligence has significantly impacted daily life through innovative applications in computer vision,¹ natural language processing,² and combinatorial optimization.³ Combinatorial optimization, particularly nondeterministic polynomial time (NP)-hard problems, spans a wide range of applications, including operations research,⁴ chip design,³ and gene sequencing.⁵ All of Karp's 21 NP-complete problems can be represented as an energy-based recurrent neural network, or Ising model.⁶

Traditionally, Ising models have been solved using conventional digital hardware, specifically, digital logic circuits based on complementary metal-oxide semiconductors. However, the computational complexity of these models has grown exponentially with their size, and conventional hardware faces significant challenges in terms of energy efficiency and footprint. Transistor scaling follows Moore's Law⁷ and Dennard scaling,⁸ but as transistors approach their physical limits, further scaling

becomes increasingly cost-ineffective. Simultaneously, the rising importance of big data and the Internet of Things (IoT) is driving a shift toward data-centric computing, challenging the architecture of digital computers where processing and storage units are physically separate. The frequent and massive data transfer between these units when solving Ising models results in substantial energy and time overheads, known as the von Neumann bottleneck. This issue is further exacerbated by the system complexity and cost involved in heterogeneously integrating artificial synapses and neurons. Consequently, an alternative computing paradigm is needed to meet the growing

Received: October 26, 2023

Revised: March 19, 2024

Accepted: April 1, 2024



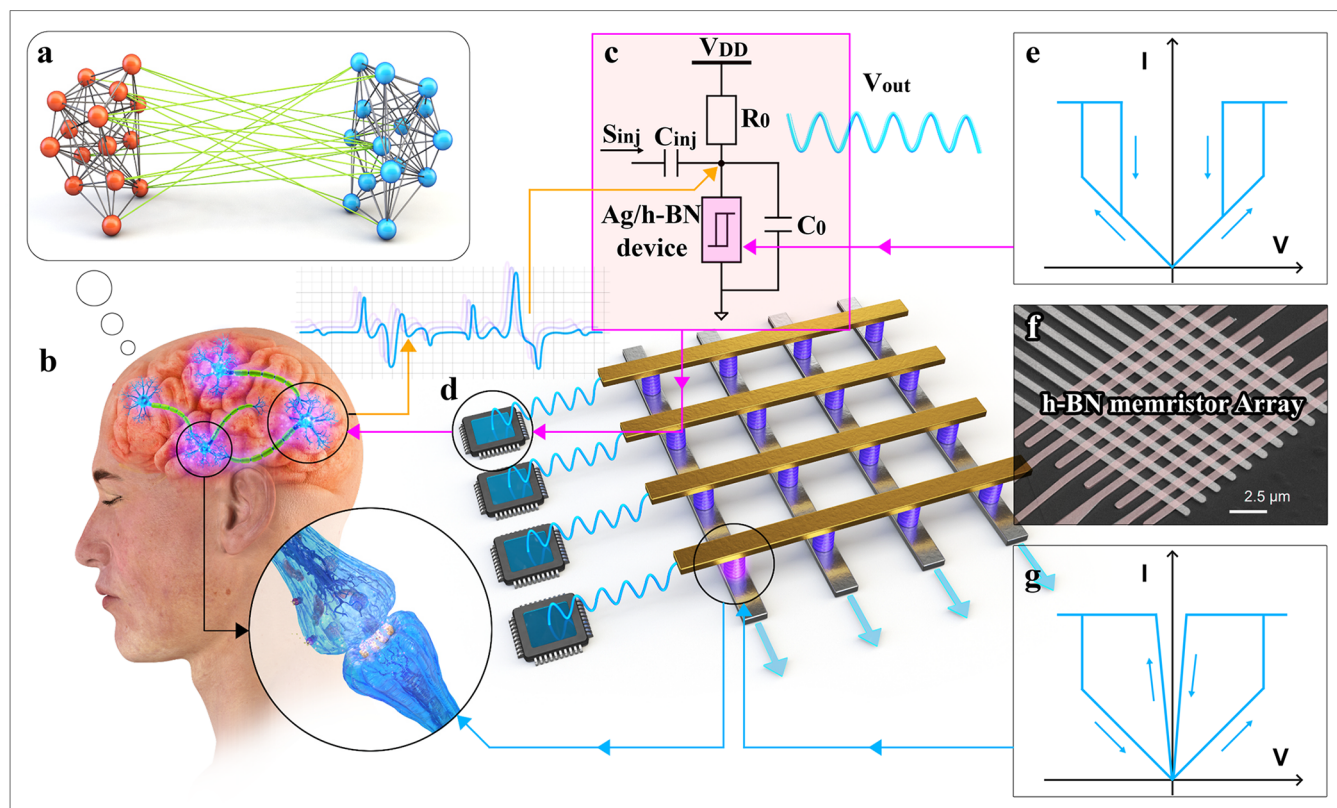


Figure 1. Brain-inspired Ising machine with retention-tunable 2D Memristors. (a) Illustration of the Max-Cut problem, a representative combinatorial optimization task where a graph is partitioned with the least remaining edges (black). (b) The combinatorial optimization problem can be solved using a brain-inspired oscillatory neural network-based Ising machine, comprised of oscillatory neurons and associated synapses. (c) The oscillatory neuron design is based on a volatile 2D Ag/h-BN/Au memristor, accompanied by a parallel capacitor C_0 , a serial resistor R_0 , and a coupling capacitor C_{inj} for injection locking. (d) A schematic illustration of the oscillatory Ising machine. The oscillatory neurons from (c) are interconnected to each other, reflecting the graph in (a), via a crossbar array of nonvolatile memristor synapses. (e) A diagram displaying the volatile $I-V$ characteristics of the 2D memristor when functioning as part of an oscillatory neuron. (f) A scanning electron micrograph (SEM) of the h-BN memristor array. (g) A diagram illustrating the nonvolatile $I-V$ characteristics of the 2D memristor when serving as synapses.

demand for computational throughput and efficiency when solving Ising models.

Various innovative hardware solutions have been proposed for solving Ising models, including optical Ising machines,⁹ quantum annealers,¹⁰ and oxide memristor-based neural networks.^{10–13} Two-dimensional material-based memristors perpetuate Moore's Law due to their ultrathin layered structure^{14–16} and 3D stackability,^{17–20} meeting the fast-growing demand for computing power for combinatorial optimization.^{21–24} Additionally, memristor crossbar arrays can naturally perform vector-matrix multiplication, one of the most computationally expensive and frequent operations in neural networks.^{25–27} The matrix is stored as the conductance of the memristor array, with Ohm's law and Kirchhoff's current law physically governing the multiplication and summation, respectively. As a result, matrix data is processed and stored in the same location, allowing processing-in-memory, which can eliminate the energy and time overheads associated with frequent data transfers in conventional digital computers based on the von Neumann architecture.^{28–30} Further, recent advances in 2D-material-based memristors, featuring rich dynamic behaviors and reduced stochasticity, enable the construction of an Ising machine with homogeneous integration of both synapses and neurons built on the same 2D memristors.³¹

Here, we report a 2D Ag/hexagonal boron nitride (h-BN)/Au memristor, which demonstrates both volatile and nonvolatile switching capabilities influenced by electrical operation parameters. We uncover the distinctive switching mechanism that enables these modes, using high-resolution transmission electron microscopy (HR-TEM). Nonvolatile memristors serve as synapses in a discrete time Hopfield neural network (HNN),^{32,33} which is capable of addressing continuous optimization problems, such as determining the minimum of quadratic polynomials, and combinatorial optimization problems, like the Max-Cut. Moreover, we demonstrate that volatile Ag/h-BN/Au memristor-based oscillators can be interconnected using nonvolatile Ag/h-BN/Au memristors to create an oscillatory Ising model. This continuous-time dynamic system addresses combinatorial optimization problems through phase synchronization and offers excellent scalability for varying problem sizes, such as Max-Cut and map coloring. Our findings on 2D memristors lay the groundwork for efficient and portable Ising machines.

RESULTS

Ising Machine with Retention-Tunable 2D Memristors. The Max-Cut problem, a key issue in combinatorial optimization, aims to divide the nodes of an undirected graph into two separate groups. The main goal is to increase the total

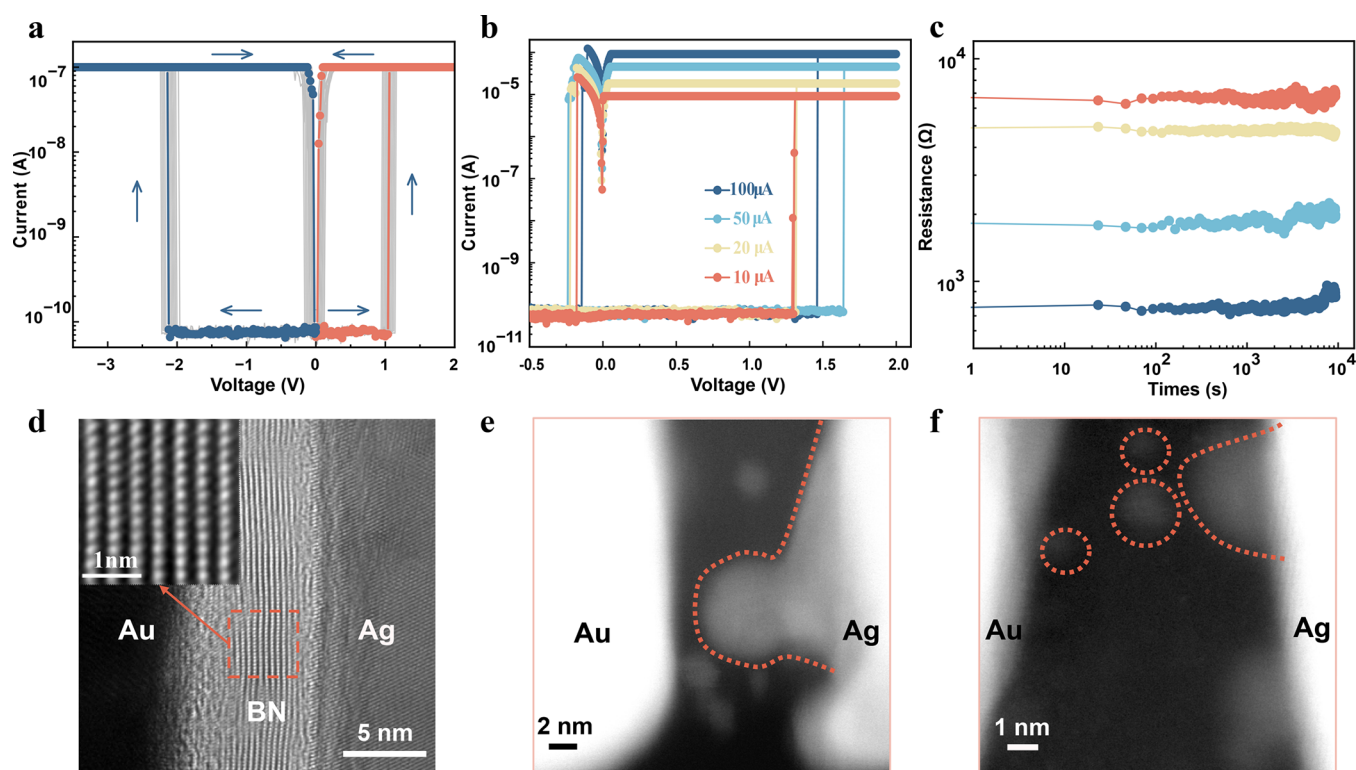


Figure 2. Memristive behaviors and In-Situ HR-TEM study of vertical Ag/h-BN/Au memristors. (a) The volatile I - V characteristics of the Ag/h-BN/Au memristor under 100 nA compliance current, exhibiting high uniformity and a large ON/OFF ratio. (b) Nonvolatile I - V characteristics under compliance currents of 10, 20, 50, and 100 μ A. The analog conductance increases proportionally with increasing compliance current. (c) Retention of different analog conductance levels at 10, 20, 50, and 100 μ A compliance, remaining stable after 10^4 s. (d) A cross-sectional transmission electron micrograph (TEM) of an Ag/h-BN/Au memristor. The inset displays a high-resolution TEM of the crystalline h-BN layer with atomic-scale spatial resolution. (e) The cross-sectional dark-field image of a nonvolatile Ag/h-BN/Au memristor in its ON-state. (f) The dark-field image of the volatile Ag/h-BN/Au memristor in its OFF-state.

weight of edges connecting these groups, as shown in Figure 1a. When applying this puzzle to the complexities of our neural structure, neurons become active by producing oscillatory signals. These signals travel through synapses to create the best possible node partition, as illustrated in Figure 1b.

To actualize this concept, an oscillator that mimics the functioning of biological neurons was carefully designed using volatile Ag/h-BN/Au devices. This simulation was achieved with the setup shown in Figure 1c, connecting a parallel capacitor and a series resistor. The role of the oscillator is to provide high processing speed and low energy use, taking advantage of the electrical properties of the Ag/h-BN memristors for oscillatory neuron activity, as shown in Figure 1e.

At the same time, synapse functionality is replicated using nonvolatile Ag/h-BN/Au memristor crossbar arrays. Figure 1f presents an SEM image of the h-BN memristor array construction, with electrode lines 1 μ m wide. Supplementary Figure 1 displays the device fabrication steps. The Ag electrodes placed at the bottom are protected from possible oxidation in air, which could otherwise impair the memristive device's performance, by h-BN passivation. Figure 1g thoroughly represents the electrical characteristics of the nonvolatile Ag/h-BN/Au devices. Figure 1d concisely presents the final hardware layout, which consists of an oscillatory neural network based on Ag/h-BN/Au devices, to address the challenges of combinatorial optimization. This design includes a combination of oscillatory neurons using volatile Ag/h-BN/Au devices on the left and nonvolatile Ag/h-BN/Au crossbar switch arrays simulating

synapses on the right. The goal of seamlessly integrating these components is to lay the foundation for bioinspired computing.

Physical Origin of Tunable Retention. The primary factor influencing the device's retention is the compliance current used during programming. When programmed with a compliance current of 10 μ A or less, the memristor's conductance experiences rapid decay over time. This instability stems from weak conductive filaments formed under low compliance currents. Ag atom surface diffusion within the filaments leads to repeatable and uniform bipolar threshold switching with a large ON/OFF ratio when subjected to a 100 nA compliance current, as illustrated in Figure 2a. Compared to volatile memristors based on mechanisms such as thermal breakdown carrier generation/recombination and metal-insulator transition, volatile devices based on the Ag filament formation and rupture mechanism exhibit both small switching speeds and large switching ratios. Compared to volatile memristors that operate on principles like thermal breakdown carrier generation/recombination and metal-insulator transition, devices utilizing the mechanism of Ag filament formation and rupture exhibit both faster switching speeds and higher switching contrasts. These characteristics confer a notable advantage in terms of minimizing noise interference, as detailed in Supplementary Table 1.

With increased compliance the memristor also exhibits nonvolatile bipolar switching and analog conductance. Figure 2b presents the voltage I - V sweeps, characterized by distinct compliance current-modulated low-resistance I - V curves (e.g., 10, 20, 50, and 100 μ A) and large ON/OFF ratio. The ON-state

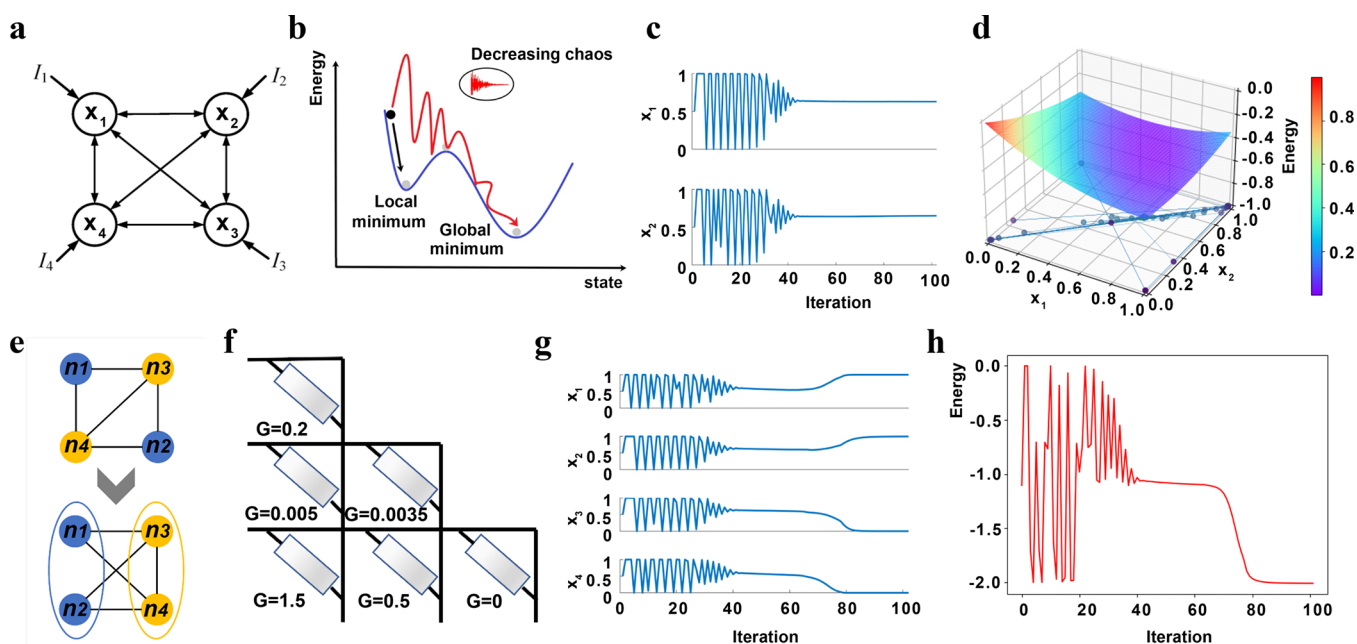


Figure 3. Experimental demonstration of a nonvolatile 2D memristor-based Hopfield network. (a) Schematic illustration of a Hopfield neural network with 4 neurons, where circles are neurons linked by bidirectional edges or synapses. (b) Schematic illustration of a possible state evolution of the Hopfield network. When the starting state is close to a local energy minimum, the state of the system can be trapped. By introducing a spontaneously convergent chaotic trajectory to the system dynamics, the network will have a larger probability of escaping from the local minimum and reaching the global minimum. (c) The neuron state trajectories in solving the continuous optimization problem using an Ag/h-BN 2D-memristor synaptic subarray to implement a 2-neuron Hopfield neural network. The two neurons eventually converge to 0.65 and 0.7, which represent the minimum of the underlying quadratic function. (d) The energy surface of the underlying quadratic function, the x_1 – x_2 plane, illustrates the network state trajectory which converges to the solution (0.65, 0.7). (e) Schematic illustration of a Max-Cut problem, which is to identify a partition of the graph where the number of weighted connections between the two subgraphs is maximized. (f) The conductance matrix of an Ag/h-BN/Au 2D-memristor synaptic subarray in solving the Max-Cut problem. (g) The associated neuron state trajectories of a 4-neuron Hopfield neural network. (h) The evolution of the Hopfield network energy as a function of the number of iterations, which gradually converges to the global minimum.

conductance increases with compliance. Figure 2c demonstrates the associated room temperature retention of the memristor when programmed with different compliance currents (e.g., 10, 20, 50, and 100 μ A), where retention time reaches 10^4 s with minimal fluctuations. Additional details on the cycle-to-cycle and device-to-device variability of memristive characteristics within the h-BN/Ag array, along with a systematic analysis of the memristor's nonvolatile and volatile properties, can be found in Supplementary Figure 2 and Figure 3.

The h-BN electrolyte is characterized by low Ag^+ ion mobility and a high Ag electrode redox rate,³⁴ resulting in a significant accumulation of Ag atoms at the cathode, which forms electrically conductive filaments. This is further supported by the asymmetric forming voltage (e.g., a significantly larger SET voltage with the Au electrode, compared to the Ag electrode).

The memristor's switching process was investigated using in situ electrical measurements with a high-resolution transmission electron microscope (HR-TEM). A focused ion beam (FIB) was employed to obtain a cross-sectional image of the Ag/h-BN/Au memristor. Figure 2d shows the h-BN layer has a well-defined lattice structure with a thickness of approximately 7 to 8 nm. This size effectively prevents critical artifacts, such as mechanical stress, contamination-induced wrinkles, and changes in lattice structure or heat confinement within the h-BN layer during the FIB process.^{35,36} The inset in Figure 2d provides a magnified view of the h-BN layer, revealing its crystalline structure.

The memristor was initially subjected to nonvolatile switching during the concurrent in situ TEM inspection. When the SET

voltage was applied to the Ag electrode, an inverted cone-shaped Ag filament was observed, extending from the anode to the cathode, as shown in Figure 2e. This occurs as Ag atoms within the electrode oxidize into Ag^+ ions, which then migrate through the h-BN layer under the influence of the electric field. Due to their relatively low mobility, these ions are reduced, forming an Ag protrusion. When a reverse voltage is applied, the conductive filament disintegrates because of the combined effects of the electric field and Joule heating^{37–39} (see Supplementary Figure 4 for the corresponding in situ nonvolatile switching I – V).

The memristor was subsequently subjected to volatile switching during in situ TEM observation. In contrast to the nonvolatile switching, continuous conductive filaments were not observed. Instead, dispersed clusters of silver were present within the BN layer, as shown in Figure 2f. Furthermore, a comparative analysis of our fabricated Ag/h-BN/Au memristor against previously documented memristors employing two-dimensional materials reveals that our device exhibits specific benefits for the development of compact and user-friendly devices. Detailed comparisons are provided in Supplementary Table 2.

2D Memristor-Based Hopfield Networks. The 2D memristors were first assessed by employing them as synapses in a Hopfield network, taking advantage of their nonvolatility. Figure 3a illustrates a Hopfield network,⁴⁰ a special type of recurrent artificial neural network, which has a nonflattened energy surface with multiple local extrema. The weight matrix of a classic Hopfield network is symmetric with zero diagonal

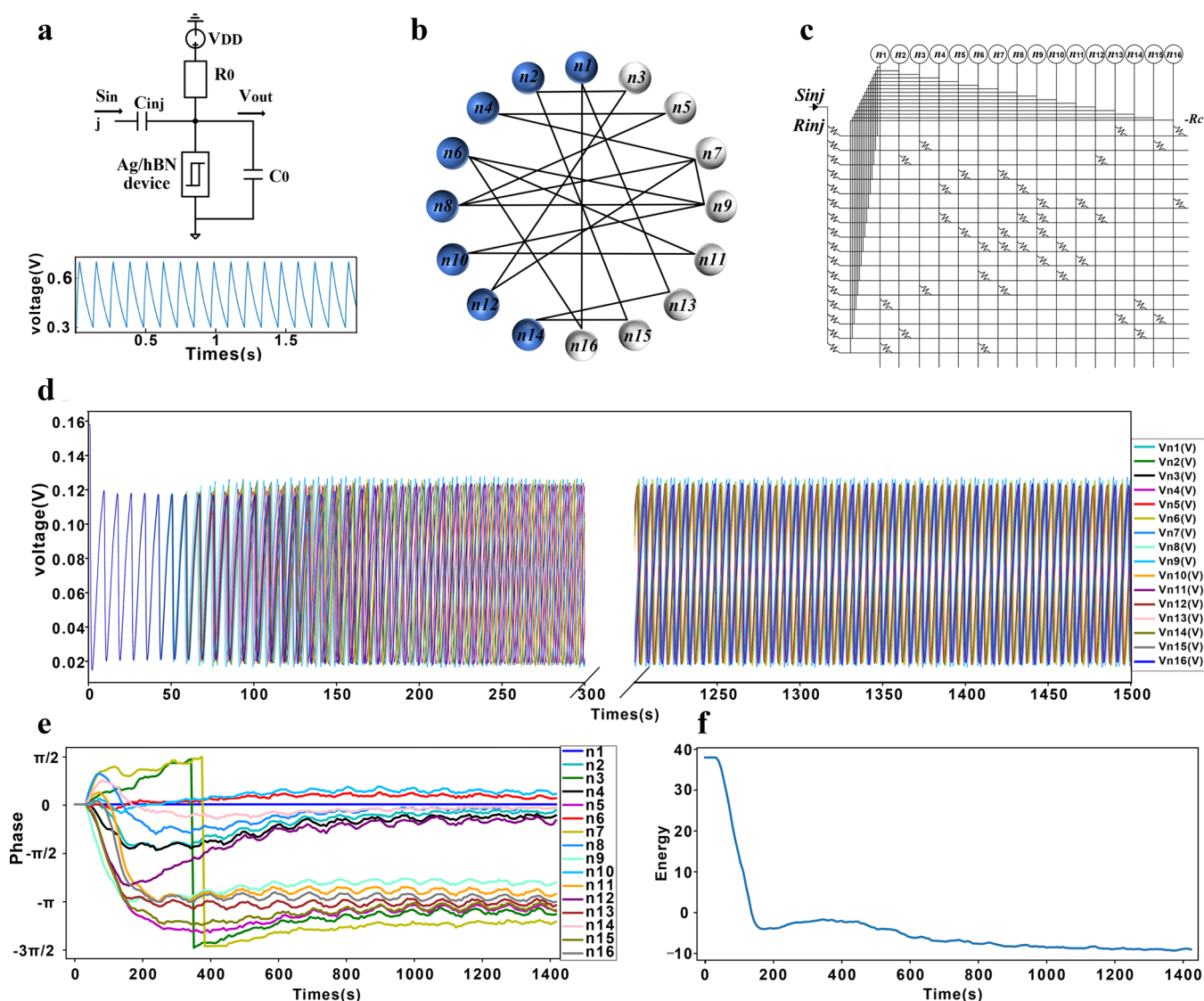


Figure 4. Simulation of a 2D-memristor-based oscillatory Ising machine for the Max-Cut problem. (a) Top: Schematic of a single oscillatory neuron consisting of a volatile 2D memristor in parallel with a capacitor C_0 and in series with a resistor R_0 , receiving a voltage bias V_{DD} . S_{inj} and C_{inj} are an injection-locking signal and injection capacitor, which imparts the oscillatory neurons with bistable phases. Bottom: The output voltage V_{out} of a single oscillatory neuron without any coupling, showing periodic oscillation at its natural frequency. (b) The Max-Cut optimization problem is physically mapped to the Ising machine consisting of 16 oscillatory neurons ($n_1 \sim n_{16}$). The oscillators are coupled using resistors R_C (of negative resistance). (c) Circuit block diagram of the oscillatory neural network-based Ising machine. The injection-locking signal S_{inj} and injection capacitor R_{inj} are used to induce the bistable oscillatory neuron phases to emulate Ising spins. (d) The output waveforms of the 16 oscillatory neurons, which are initially synchronized. Subsequently, they become desynchronized due to the injection-locking signal, as they search for optimal phases. Eventually, the waveforms converge into two distinct groups. (e) Top: the evolution of the phases of the 16 neurons over the optimization. The phases either converge to in-phase or out-of-phase with respect to the inject signal, indicating the partition of the graph or the solution of the Max-Cut problem. (f) The evolution of the energy of the Ising machine. As the phase of the neuron converges, the energy represented by the system gradually converges to the global minimum.

elements. Thus, the neurons do not have self-feedback to keep the network stable. The HNN with self-feedback reduces its energy monotonically starting from the initial state (shown in Figure 3b). However, being trapped in a local minimum impedes solving an optimization problem. To increase the chances of reaching the global minimum, the network needs to escape from such local minima. A very effective method is to add appropriate self-feedback to the neurons of the Hopfield network to introduce transient chaotic behaviors,⁴ where the dynamics of the network follow the equations defined in Methods.

A Hopfield network with transient chaotic dynamics was experimentally implemented using 2D memristor synapses to

solve a representative continuous optimization problem, finding the minimum of a quadratic function, and a combinatorial optimization problem, the Max-Cut. For the continuous minimization problem, the goal was to find the minimum of a quadratic function that is mapped to the energy function of the network. The corresponding synaptic weights of the Hopfield network were designed according to the differential equation $\frac{\partial E}{\partial x_i} = \sum_j \left(-\frac{1}{2} W_{ij} x_j + \theta_i \right)$, where E is the quadratic energy function to be minimized; W_{ij} is the synaptic strength between the i -th preneuron and the j -th postneuron; x_j is the output of the j -th neuron, while θ_i is the threshold of the i -th neuron.

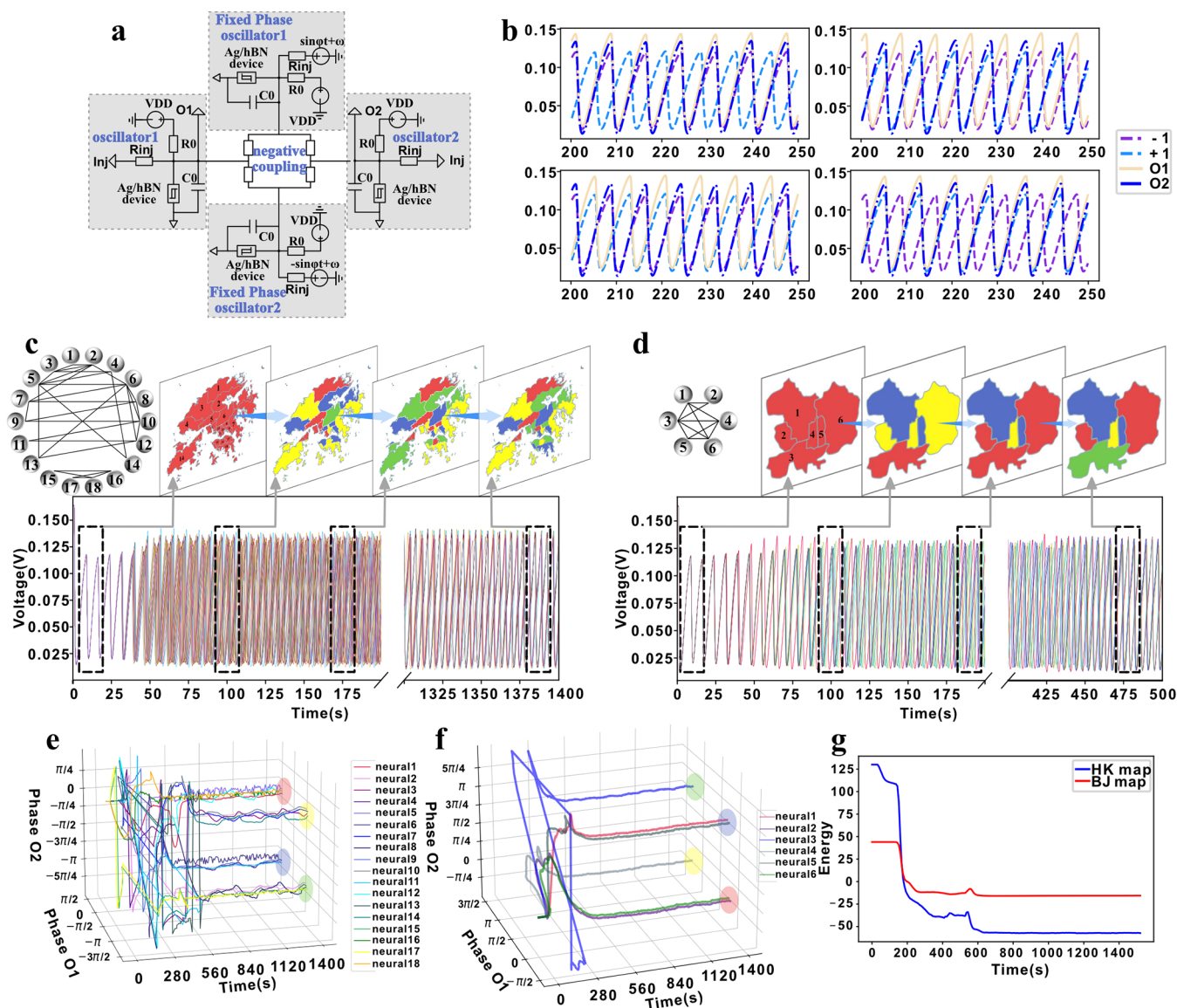


Figure 5. Simulation of map coloring using a 2D memristor-based oscillatory Ising machine. (a) Schematic diagram of a single coloring neuron, which is composed of two free-phase oscillators and two fixed-phase oscillators. The two free-phase oscillators serve as the output (O1 and O2) of the neuron, while the fixed-phase oscillators provide the reference phases of +1 (above) and -1 (below). (b) Output voltages O1 and O2 of a single coloring neuron and intraneuron reference phases -1 and +1, showing four stable states corresponding to the four mapping colors. That is, the phases of O1 and O2 are -1 and -1 (top left, red), -1 and +1 (top right, blue), +1 and -1 (bottom left, yellow), +1 and +1 (bottom right, green). (c, d) Hong Kong and Beijing map coloring problems. The upper left panels show the equivalent graph representation of the maps, where each node corresponds to a region of the map and neighboring regions are nodes with an edge. The color of nodes is represented by the states of the oscillatory neuron in (b). The evolution of map coloring is shown in the upper left, which corresponds to the four boxes in the V-t diagram below. (e, f) Neuron states in the Hong Kong and Beijing map coloring problem. These neuron states quickly diversified after the starting the optimization, searching the phase space, which finally converge to four areas, representing four different colors, thus completing the map coloring problem. (g) The evolution of the energy of the Ising machine.

Here, we use $E = f(x_1, x_2) = 0.4x_1^2 + 0.2x_2^2 - 0.8x_1 - 0.54x_2 + 0.4x_1x_2$ as an example, which depends on the two variables x_1 and x_2 in a 2D space for better visualization. The corresponding memristor conductance is iteratively programmed into the 2D memristor synaptic array, while neuron bias is implemented in software (see Supplementary Figure 5 on the memristor-based hardware HNN setup). Figure 3c shows the corresponding state evolution. The network reaches the optimal solution after the collapse of the chaos. The final states of the neurons precisely converged to 0.65 and 0.7, respectively, as shown in Figure 3d, illustrating the energy surface and the evolution path in the 2D space (see Supplementary Figure 6 for another example of

solving a continuous optimization problem). In instances where HNN is employed to tackle continuous optimization problems without the integration of convergent chaotic signals, the number of time steps required to reach the optimal solution is significantly higher. These experimental outcomes are documented in Supplementary Figure 7.

In addition to continuous optimization problems, we used the 2D memristor-based Hopfield network to solve a representative combinatorial optimization problem, the Max-Cut problem. In the Max-Cut problem, the optimization goal is to find the division of a given graph to divide all nodes into two groups to maximize the weighted connections between them (Figures 1a

and 3e). We employed analog weights in this problem setting, which differs from the simple Max-Cut problem with binary edge weights. Because the weight matrix of the Hopfield network is symmetric with zero diagonal elements, we used the lower triangular matrix of the weights which were physically mapped to a 3×3 Ag/h-BN/Au memristor subarray to solve the 4-node Max-Cut problem shown in Figure 3f. Figure 3g shows that the state of each neuron evolves over the iterations, which gradually converges to the optimal value after the chaos diminishes. The final network configuration indicates that nodes 1 and 2 are within the same partition, and nodes 3 and 4 are with the other partition. Figure 3h shows the evolution of the network energy. It can be clearly seen in the figure that the energy of the network gradually drops to the global minimum as the number of iterations increases. The performance of HNN in solving combinatorial optimization problems is sensitive to the presence of chaotic signals. If an excessive amount of chaotic signals were introduced or if they are completely omitted, the HNN is at risk of converging to a local optimum, thereby failing to find the correct solution. This behavior is illustrated and discussed in Supplementary Figures 8, 9, and 10. Supplementary Tables 3 and 4 display the time consumption, power consumption, and latency of the mem-HNN system, respectively.

2D Memristor-Based Oscillatory Ising Machines. In addition to serving the nonvolatile synaptic weights in the Ising model, 2D Ag/h-BN/Au memristors can work as oscillatory neurons in an oscillator-based Ising machine, which leverages their volatility.⁴¹ Figure 4a shows a circuit schematic of the Ag/h-BN/Au memristor-based oscillatory neuron. A constant bias voltage ($V_{DD} = 0.28$ V) makes it operate in a locally active domain, while R_0 and C_0 are the resistor in series and the capacitor in parallel with the volatile 2D memristor, respectively. The simulated output waveform of a standalone oscillatory neuron is shown in the lower panel of Figure 4a.

Figure 4b depicts a graph Max-Cut problem, which consists of 16 nodes, with colors indicating the optimal solution, and associated edges. The graph is physically mapped to the oscillator neural network-based Ising machine, as indicated by the circuit diagram in Figure 4c. The hardware oscillatory Ising machine consists of both nonvolatile 2D memristor-based synapses and volatile 2D memristor-based oscillatory neurons (see Methods for details of negative coupling connections).

To represent Ising spins using bistable phases of oscillatory neurons, an external sinusoidal signal S_{inj} is used for injection-locking. When $S_{inj} = 0$, the oscillators in the network will eventually be synchronized. When S_{inj} is a sine wave of twice the natural frequency of the oscillatory neuron, the oscillators will exhibit two steady-state phases (0 or π) under the appropriate choices of C_{inj} and R_C . This is consistent with the simulated temporal waveform and phase of the oscillatory neurons in Figure 4d and e, respectively.

Upon the start of network evolution, the neuronal phases rapidly diverge, essentially executing a 16-dimensional search for the optimal solution to the Max-Cut problem, as depicted in Figure 4d,e. Subsequently, the neuronal phases gradually stabilize under the influence of the injection signal, driven by system energy minimization, as demonstrated in Figure 4f, a process akin to simulated annealing. Consequently, the neurons' phases ultimately segregate into two categories, in-phase and out-of-phase, signifying the ideal node partition for the Max-Cut problem, as illustrated in Figure 4e.

Supplementary Figure 12 presents an analysis of the energy consumption for an Oscillator Neural Network (ONN) tasked

with a 4-neuron Max-Cut problem. It reveals that the energy usage of both volatile and nonvolatile memristors constitutes only a minor fraction of the total system energy consumption. Notably, there is an inverse relationship between the overall system energy consumption and the oscillation frequency of the oscillators. Furthermore, Supplementary Table 5 provides a detailed comparison of key performance metrics such as clock frequency, annealing time, problem-solving duration, and energy usage between memristor-based Hopfield Neural Networks (mem-HNN), memristor-based Oscillator Neural Networks (mem-ONN), and the current leading annealing accelerators.

Oscillator Neural Network for Map Coloring Problem.

Another exemplary combinatorial optimization problem is map coloring, which can be hardware-mapped onto the 2D memristor-based oscillatory Ising machine. The objective of this optimization task is to color an arbitrary map using the fewest possible colors, ensuring that no two adjacent regions have the same color. Mathematically, it has been proven that the maximum number of colors required does not exceed four.

To address the map coloring problem, a 4-oscillator neuron circuit was designed to represent the four potential colors for a specific region on the map, as illustrated in Figure 5a. This circuit consists of two free-phase 2D memristor oscillators and two fixed-phase 2D memristor oscillators, which are fully interconnected. There is a 180° phase difference between the two fixed-phase oscillators, symbolizing two states of +1 and -1. This enables the neuron to possess four stable states, representing four distinct colors, as illustrated in Figure 5b. The two spins for the i -th neuron are S_{01i} and S_{02i} . The $W_{ij} = 1$ indicates that there is a connection between the i -th neuron and the j -th neuron, and 0 if otherwise (see the Methods for the corresponding Hamiltonian function).

We utilized both Hong Kong and Beijing maps for coloring with the oscillatory Ising machine. The maps were first converted into graphs, as shown in Figure 5c,d, where each node represents a region on the map, and neighboring regions correspond to graph nodes sharing edges. The graph was then mirrored onto the oscillatory Ising machine topology, with nodes and edges mapped to volatile oscillatory neurons and nonvolatile synapses, respectively (refer to Methods for details on negative coupling connections).

The temporal waveform of the oscillatory neurons and associated map colors for Hong Kong and Beijing maps are displayed in Figure 5c and d, respectively. At the start of network evolution, the injection locking signal is absent, causing all neurons to synchronize and all regions of both maps to initially share the same red color. Over time, the injection locking signal desynchronizes the oscillators, leading to the diversification of map colors and a search for the configuration that minimizes the system energy (e.g., Hamiltonian function) in the phase space, as shown in Figure 5c,g. Eventually, the oscillator phases converge to in-phase and out-phase groups. As a result, the neuron states (each state is collectively represented by the phases of the two free oscillators) converge to one of the four map colors, as depicted in the 3D neural state evolutionary diagrams in Figure 5e,f. The resulting colored maps correspond to the optimal solutions where distinct colors for neighboring regions minimize the system energy (see Supplementary Figure 13 for an additional example of solving a map coloring problem in Daejeon).

CONCLUSIONS

In this study, we showcased in-memory computing using an oscillatory Ising machine with 2D memristors, which exhibit both volatile and nonvolatile resistive switching modulated by electrical operating conditions. The HR-TEM observation revealed the rich underlying ion dynamics responsible for tunable retention. The nonvolatile 2D memristors function as synapses in a HNN, solving continuous optimization problems (e.g., finding the minimum of a quadratic polynomial) and combinatorial optimization problems (e.g., the Max-Cut) in discrete time steps. Furthermore, volatile 2D memristor-based oscillatory neurons can be interconnected through nonvolatile 2D memristor synapses in an oscillatory Ising machine. This machine addresses combinatorial optimization (e.g., Max-Cut and map coloring) in a continuous way using phase synchronization, thereby eliminating the need for cumbersome analog-digital conversion. Our 2D memristors give a hint on the development of efficient and portable Ising machines.

METHODS

Device Fabrication. A 300 nm thick SiO₂/Si wafer was chosen as the substrate of our Ag/h-BN/Au memristor device. First, a Cr/Au(5/50 nm) electrode array was deposited on the SiO₂/Si substrate. Then, we exfoliated h-BN flakes mechanically from a bulk Taniguchi's h-BN crystal. We transferred them to a substrate coated with PVA and PMMA. The substrate was coated with PVA and PMMA at 4000 rpm for 60 s and annealed at 373 K for 1 min. We transferred the h-BN onto the Au electrode array using the dry transfer method. The thickness of the h-BN was 7–8 nm. Then, we deposited a Ag (50 nm) electrode array on the h-BN/Au substrate. We deposited the metals (Cr, Ag, and Au) using a thermal evaporator and patterned the array design based on the substrate using e-beam lithography and the lift-off process. A positive e-beam resist layer was coated by e-beam resist (PMMA A4) at 4000 rpm for 60 s and baked at 433 K for 3 min. The electrodes of the samples were exposed to an e-beam for 1 min, and the pads were exposed for 5 min with an e-beam lithography machine (Nanometer Pattern Generation System for JSM-6510, JEOL). The samples were patterned with a MIBK (methyl isobutyl ketone) developer solution. Acetone was used for the lift-off process.

TEM Characterization. SAED, HRTEM, and EDS data were collected by double aberration corrected TEM under 300 kV (Thermo Fisher Scientific, Titan Themis Z). Specimens were picked from the switched devices with the focused ion beam method (Thermo Fisher Scientific, Helios G4 UC). The ion beam was set at 30 kV, 0.23 nA, and 80 pA for milling, and 5 kV, 40 pA, and 15 pA for cleaning.

Experimental Implementation of a Hopfield Network. For the continuous optimization problem, the synaptic weights of the 2×2 Ag/h-BN/Au memristor array were designed to be 1.25, 2.5, 2.5, and 2.5 k Ω . The bias of the neurons was set at 0.8 and 0.54, and were implemented in the software. The synaptic weights for the combinatorial optimization problem are shown in Figure 3f. The targeted conductance matrices were iteratively programmed into the memristor arrays using an Agilent B1500 semiconductor parameter analyzer. The forward pass of the Hopfield network began by sourcing voltages to the Ag/h-BN/Au memristor array using a Rigol 4162 two channel waveform generator. The output currents of the array were concurrently sampled by multiple B1511 modules of the Agilent B1500. All the rest of the operations were carried by a digital computer.

The neurons of the Hopfield network were simulated in software according to the following equations.

$$x_i(t) = \frac{1}{1 + e^{-y_i/\epsilon}}$$

$$y_i(t+1) = ky_i(t) + \alpha \left(\sum_{j=1}^n w_{ij}x_j(t) + I_i \right) + z_i(t)(x_i(t) - I_0)$$

$$z_i(t+1) = (1 - \beta)z_i(t)$$

Here x_i , y_i , and z_i are defined as the neural output, the internal membrane potential of the neuron, and the self-feedback weight of neuron i , respectively, following the definition in ref 4. The neural output x_i depends on the internal membrane potential of neuron y_i as a sigmoid function with a steepness parameter ϵ . The membrane potential y_i at the next time step is codetermined by 3 factors, the current membrane potential modulated by a leaky factor k , the weighted stimulus (scaled by the factor α) received by the neuron from neighbors and the external input I_i , and the self-feedback to induce transient chaos. For the self-feedback term, I_0 is a positive constant affecting the self-feedback strength, and z_i exponentially decays with a damping parameter β .

Simulated Oscillatory Neural Network. The operation of the oscillatory neural network-based Ising machine was simulated using experimentally extracted device parameters in LTSpice. Here, C_{inj} was set to 5 nF, while R_C was set to -5 M Ω . (The negative coupling resistance can be physically implemented using an analog inverter, which is shown in Supplementary Figure 11.)

The corresponding Hamiltonian function of the map coloring problem in the simulated oscillatory neural network is provided.

$$H = \sum_{i \neq j} W_{ij} S_{O1i} S_{O1j} + W_{ij} S_{O2i} S_{O2j}$$

ASSOCIATED CONTENT

Supporting Information

The Supporting Information is available free of charge at <https://pubs.acs.org/doi/10.1021/acsnano.3c10559>.

Additional figures and tables that enhance understanding of Ag/h-BN/Au memristive device research, detailing fabrication, performance variability, Hopfield Neural Networks operations, optimization uses, chaotic signals impact, and negative resistance coupling. Tables compare device specs, mem-HNN and mem-ONN performance metrics, and benchmarks against leading annealing accelerators (PDF)

AUTHOR INFORMATION

Corresponding Authors

Linfeng Sun — Centre for Quantum Physics, Key Laboratory of Advanced Optoelectronic Quantum Architecture and Measurement (MOE), School of Physics, Beijing Institute of Technology, Beijing 100081, China; Email: sunlinfeng@bit.edu.cn

Zhongrui Wang — Department of Electrical and Electronic Engineering, The University of Hong Kong, Hong Kong, China; Email: zrwang@eee.hku.hk

Heejun Yang — Department of Physics, Korea Advanced Institute of Science and Technology (KAIST), Daejeon 34141, Korea; orcid.org/0000-0003-0502-0054; Email: h.yang@kaist.ac.kr

Authors

Xi Chen — Centre for Quantum Physics, Key Laboratory of Advanced Optoelectronic Quantum Architecture and Measurement (MOE), School of Physics, Beijing Institute of Technology, Beijing 100081, China; Department of Electrical

and Electronic Engineering, The University of Hong Kong, Hong Kong, China

Dongliang Yang – Centre for Quantum Physics, Key Laboratory of Advanced Optoelectronic Quantum Architecture and Measurement (MOE), School of Physics, Beijing Institute of Technology, Beijing 100081, China

Geunwoo Hwang – Division of Chemical Engineering and Materials Science, Graduate Program in System Health Science and Engineering, Ewha Womans University, Seoul 03760, Korea

Yujiao Dong – Department of Electrical and Electronic Engineering, The University of Hong Kong, Hong Kong, China; Institute of Modern Circuit and Intelligent Information, Hangzhou Dianzi University, Hangzhou 310018, China

Binbin Cui – Department of Electrical and Electronic Engineering, The University of Hong Kong, Hong Kong, China

Dingchen Wang – Department of Electrical and Electronic Engineering, The University of Hong Kong, Hong Kong, China

Hegan Chen – Department of Electrical and Electronic Engineering, The University of Hong Kong, Hong Kong, China

Ning Lin – Department of Electrical and Electronic Engineering, The University of Hong Kong, Hong Kong, China

Wenqi Zhang – Department of Biomedical Engineering, City University of Hong Kong, Hong Kong, China

Huihan Li – Centre for Quantum Physics, Key Laboratory of Advanced Optoelectronic Quantum Architecture and Measurement (MOE), School of Physics, Beijing Institute of Technology, Beijing 100081, China

Ruiwen Shao – Beijing Advanced Innovation Center for Intelligent Robots and Systems and Institute of Engineering Medicine, Beijing Institute of Technology, Beijing 100081, China

Peng Lin – College of Computer Science and Technology, Zhejiang University, Hang Zhou 310013, China

Heemyoung Hong – Department of Physics, Korea Advanced Institute of Science and Technology (KAIST), Daejeon 34141, Korea

Yugui Yao – Centre for Quantum Physics, Key Laboratory of Advanced Optoelectronic Quantum Architecture and Measurement (MOE), School of Physics, Beijing Institute of Technology, Beijing 100081, China; orcid.org/0000-0003-3544-3787

Complete contact information is available at:

<https://pubs.acs.org/10.1021/acsnano.3c10559>

Author Contributions

[#]These authors contributed equally to this work (X.C., D.Y., and G.H.).

Notes

The authors declare no competing financial interest.

ACKNOWLEDGMENTS

This work was supported by National Key R&D Plan (2022YFA1405600) and the Samsung Research Funding and Incubation Center of Samsung Electronics under Project No. SRFC-MA1701-S2, and Z.W. thanks the support from Hong Kong Research Grant Council - Early Career Scheme (Grant No. 27206321) and National Natural Science Foundation of China - Excellent Young Scientists Fund (Hong Kong and Macau; Grant No. 62122004). This research is also supported by Beijing Natural Science Foundation (Grant No. Z210006) and ACCESS – AI Chip Center for Emerging Smart Systems,

sponsored by Innovation and Technology Fund (ITF), Hong Kong SAR.

REFERENCES

- (1) Bengio, Y.; Lodi, A.; Prouvost, A. Machine learning for combinatorial optimization: A methodological tour d'horizon. *European Journal of Operational Research* **2021**, *290* (2), 405–421.
- (2) Mirhoseini, A.; Goldie, A.; Yazgan, M.; Jiang, J. W.; Songhori, E.; Wang, S.; Lee, Y.-J.; Johnson, E.; Pathak, O.; Nazi, A.; et al. A graph placement methodology for fast chip design. *Nature* **2021**, *594* (7862), 207–212.
- (3) Naseri, G.; Koffas, M. A. G. Application of combinatorial optimization strategies in synthetic biology. *Nat. Commun.* **2020**, *11* (1), 2446.
- (4) Yang, K.; Duan, Q.; Wang, Y.; Zhang, T.; Yang, Y.; Huang, R. Transiently chaotic simulated annealing based on intrinsic nonlinearity of memristors for efficient solution of optimization problems. *Science Advances* **2020**, *6* (33), No. eaba9901.
- (5) Ising, E. Beitrag zur Theorie des Ferromagnetismus. *Zeitschrift für Physik* **1925**, *31* (1), 253–258.
- (6) Brush, S. G. History of the Lenz-Ising Model. *Rev. Mod. Phys.* **1967**, *39* (4), 883–893.
- (7) Hamerly, R.; Inagaki, T.; McMahon, P. L.; Venturelli, D.; Marandi, A.; Onodera, T.; Ng, E.; Langrock, C.; Inaba, K.; Honjo, T.; et al. Experimental investigation of performance differences between coherent Ising machines and a quantum annealer. *Science Advances* **2019**, *5* (5), eaau0823.
- (8) Shin, J. H.; Jeong, Y. J.; Zidan, M. A.; Wang, Q.; Lu, W. D. Hardware Acceleration of Simulated Annealing of Spin Glass by RRAM Crossbar Array. *2018 IEEE International Electron Devices Meeting (IEDM)* **2018**, 3.3.1–3.3.4.
- (9) Mahmoodi, M. R.; Prezioso, M.; Strukov, D. B. Versatile stochastic dot product circuits based on nonvolatile memories for high performance neurocomputing and neurooptimization. *Nat. Commun.* **2019**, *10* (1), 5113.
- (10) Cai, F.; Kumar, S.; Van Vaerenbergh, T.; Sheng, X.; Liu, R.; Li, C.; Liu, Z.; Foltin, M.; Yu, S.; Xia, Q.; et al. Power-efficient combinatorial optimization using intrinsic noise in memristor Hopfield neural networks. *Nature Electronics* **2020**, *3* (7), 409–418.
- (11) Dutta, S.; Khanna, A.; Assoa, A.; Paik, H.; Schlom, D. G.; Toroczka, Z.; Raychowdhury, A.; Datta, S. An Ising Hamiltonian solver based on coupled stochastic phase-transition nano-oscillators. *Nature Electronics* **2021**, *4* (7), 502–512.
- (12) Wang, Z.; Li, C.; Song, W.; Rao, M.; Belkin, D.; Li, Y.; Yan, P.; Jiang, H.; Lin, P.; Hu, M.; et al. Reinforcement learning with analogue memristor arrays. *Nature Electronics* **2019**, *2* (3), 115–124.
- (13) Yang, Y.; Huang, R. Probing memristive switching in nanoionic devices. *Nature Electronics* **2018**, *1* (5), 274–287.
- (14) Liu, C.; Chen, H.; Wang, S.; Liu, Q.; Jiang, Y.-G.; Zhang, D. W.; Liu, M.; Zhou, P. Two-dimensional materials for next-generation computing technologies. *Nat. Nanotechnol.* **2020**, *15* (7), 545–557.
- (15) Sun, L.; Zhang, Y.; Hwang, G.; Jiang, J.; Kim, D.; Eshete, Y. A.; Zhao, R.; Yang, H. Synaptic Computation Enabled by Joule Heating of Single-Layered Semiconductors for Sound Localization. *Nano Lett.* **2018**, *18* (5), 3229–3234.
- (16) Wang, L.; Meric, I.; Huang, P. Y.; Gao, Q.; Gao, Y.; Tran, H.; Taniguchi, T.; Watanabe, K.; Campos, L. M.; Muller, D. A.; et al. One-Dimensional Electrical Contact to a Two-Dimensional Material. *Science* **2013**, *342* (6158), 614–617.
- (17) Sun, L.; Zhang, Y.; Han, G.; Hwang, G.; Jiang, J.; Joo, B.; Watanabe, K.; Taniguchi, T.; Kim, Y.-M.; Yu, W. J.; et al. Self-selective van der Waals heterostructures for large scale memory array. *Nat. Commun.* **2019**, *10* (1), 3161.
- (18) Guo, H.-W.; Hu, Z.; Liu, Z.-B.; Tian, J.-G. Stacking of 2D Materials. *Adv. Funct. Mater.* **2021**, *31* (4), No. 2007810.
- (19) Sung, S. H.; Schnitzer, N.; Brown, L.; Park, J.; Hovden, R. Stacking, strain, and twist in 2D materials quantified by 3D electron diffraction. *Physical Review Materials* **2019**, *3* (6), No. 064003.

- (20) Briggs, N.; Subramanian, S.; Lin, Z.; Li, X.; Zhang, X.; Zhang, K.; Xiao, K.; Geoghegan, D.; Wallace, R.; Chen, L.-Q.; et al. A roadmap for electronic grade 2D materials. *2D Materials* **2019**, *6* (2), 022001.
- (21) Loan, P. T. K.; Zhang, W.; Lin, C. T.; Wei, K. H.; Li, L. J.; Chen, C. H. Graphene/MoS₂ heterostructures for ultrasensitive detection of DNA hybridisation. *Advanced materials* **2014**, *26* (28), 4838–4844.
- (22) Geim, A. K.; Grigorieva, I. V. Van der Waals heterostructures. *Nature* **2013**, *499* (7459), 419–425.
- (23) Huh, W.; Lee, D.; Lee, C. H. Memristors based on 2D materials as an artificial synapse for neuromorphic electronics. *Adv. Mater.* **2020**, *32* (51), No. 2002092.
- (24) Li, H.; Wang, S.; Zhang, X.; Wang, W.; Yang, R.; Sun, Z.; Feng, W.; Lin, P.; Wang, Z.; Sun, L.; et al. Memristive Crossbar Arrays for Storage and Computing Applications. *Advanced Intelligent Systems* **2021**, *3* (9), No. 2100017.
- (25) Xie, Z.; Zhuge, C.; Zhao, Y.; Xiao, W.; Fu, Y.; Yang, D.; Zhang, S.; Li, Y.; Wang, Q.; Wang, Y.; et al. All-Solid-State Vertical Three-Terminal N-Type Organic Synaptic Devices for Neuromorphic Computing. *Adv. Funct. Mater.* **2022**, *32* (21), 2107314.
- (26) Wang, S.; Li, Y.; Wang, D.; Zhang, W.; Chen, X.; Dong, D.; Wang, S.; Zhang, X.; Lin, P.; Gallicchio, C.; et al. Echo state graph neural networks with analogue random resistive memory arrays. *Nature Machine Intelligence* **2023**, *5* (2), 104–113.
- (27) Midya, R.; Wang, Z.; Asapu, S.; Zhang, X.; Rao, M.; Song, W.; Zhuo, Y.; Upadhyay, N.; Xia, Q.; Yang, J. J. Reservoir Computing Using Diffusive Memristors. *Advanced Intelligent Systems* **2019**, *1* (7), No. 1900084.
- (28) Kumar, S.; Williams, R. S.; Wang, Z. Third-order nanocircuit elements for neuromorphic engineering. *Nature* **2020**, *585* (7826), 518–523.
- (29) Li, D.; Liang, X. *Neurons Mimicked by Electronics*; Nature Publishing Group: UK London, 2018. DOI: 10.1038/d41586-018-02025-x.
- (30) Sun, L.; Wang, Z.; Jiang, J.; Kim, Y.; Joo, B.; Zheng, S.; Lee, S.; Yu, W. J.; Kong, B.-S.; Yang, H. In-sensor reservoir computing for language learning via two-dimensional memristors. *Science Advances* **2021**, *7* (20), No. eabg1455.
- (31) Wang, M.; Cai, S.; Pan, C.; Wang, C.; Lian, X.; Zhuo, Y.; Xu, K.; Cao, T.; Pan, X.; Wang, B.; et al. Robust memristors based on layered two-dimensional materials. *Nature Electronics* **2018**, *1* (2), 130–136.
- (32) Wang, Z.; Joshi, S.; Savel'ev, S. E.; Jiang, H.; Midya, R.; Lin, P.; Hu, M.; Ge, N.; Strachan, J. P.; Li, Z.; et al. Memristors with diffusive dynamics as synaptic emulators for neuromorphic computing. *Nature Materials* **2017**, *16* (1), 101–108.
- (33) Shi, Y.; Liang, X.; Yuan, B.; Chen, V.; Li, H.; Hui, F.; Yu, Z.; Yuan, F.; Pop, E.; Wong, H. S. P.; et al. Electronic synapses made of layered two-dimensional materials. *Nature Electronics* **2018**, *1* (8), 458–465.
- (34) Yang, Y.; Gao, P.; Li, L.; Pan, X.; Tappertzhofen, S.; Choi, S.; Waser, R.; Valov, I.; Lu, W. D. Electrochemical dynamics of nanoscale metallic inclusions in dielectrics. *Nat. Commun.* **2014**, *5* (1), 4232.
- (35) Sun, L.; Hwang, G.; Choi, W.; Han, G.; Zhang, Y.; Jiang, J.; Zheng, S.; Watanabe, K.; Taniguchi, T.; Zhao, M.; et al. Ultralow switching voltage slope based on two-dimensional materials for integrated memory and neuromorphic applications. *Nano Energy* **2020**, *69*, No. 104472.
- (36) Lanza, M.; Wong, H.-S. P.; Pop, E.; Ielmini, D.; Strukov, D.; Regan, B. C.; Larcher, L.; Villena, M. A.; Yang, J. J.; Goux, L.; et al. Recommended Methods to Study Resistive Switching Devices. *Advanced Electronic Materials* **2019**, *5* (1), No. 1800143.
- (37) Yang, D.; Yang, H.; Guo, X.; Zhang, H.; Jiao, C.; Xiao, W.; Guo, P.; Wang, Q.; He, D. Robust polyethylenimine electrolyte for high performance and thermally stable atomic switch memristors. *Adv. Funct. Mater.* **2020**, *30* (50), No. 2004514.
- (38) Yang, J. J.; Strukov, D. B.; Stewart, D. R. Memristive devices for computing. *Nature Nanotechnol.* **2013**, *8* (1), 13–24.
- (39) You, B. K.; Park, W. I.; Kim, J. M.; Park, K.-I.; Seo, H. K.; Lee, J. Y.; Jung, Y. S.; Lee, K. J. Reliable control of filament formation in resistive memories by self-assembled nanoinsulators derived from a block copolymer. *ACS Nano* **2014**, *8* (9), 9492–9502.
- (40) Hopfield, J. J. Neural networks and physical systems with emergent collective computational abilities. *Proc. Natl. Acad. Sci. U. S. A.* **1982**, *79* (8), 2554–2558.
- (41) Wang, T.; Roychowdhury, J. OIM: Oscillator-Based Ising Machines for Solving Combinatorial Optimisation Problems. *Lecture Notes in Computer Science* **2019**, *11493*, 232–256.